



The fingerprint of a flow: wrinkle patterns in non-uniform coatings on pre-stretched soft foundations

Journal:	<i>Soft Matter</i>
Manuscript ID	SM-ART-10-2018-002057.R1
Article Type:	Paper
Date Submitted by the Author:	16-Dec-2018
Complete List of Authors:	Schleifer, Jonathan; Princeton University Department of Chemical and Biological Engineering Marthelot, Joel; Princeton University Department of Chemical and Biological Engineering Jones, Trevor; Princeton University Department of Chemical and Biological Engineering Brun, Pierre-Thomas; Princeton University Department of Chemical and Biological Engineering

Cite this: DOI: 10.1039/xxxxxxxxxx

The fingerprint of a flow: wrinkle patterns in non-uniform coatings on pre-stretched soft foundations

J. Schleifer,^a J. Marthelot,^a T.J. Jones,^a and P.-T. Brun^{a*}Received Date
Accepted Date

DOI: 10.1039/xxxxxxxxxx

www.rsc.org/journalname

We study the wrinkle patterns obtained when applying a thin polymeric film on a uniaxially pre-stretched soft foundation. The film is coated onto a substrate where it drains under the action of gravity, thereby introducing a continuous variation in its thickness. We first study the fluid mechanics component of the problem and derive the coating profile as a function of the curing properties of the polymeric solution. Upon polymerization, the prestretch is released and yields the formation of wrinkles, which arrange in organized patterns, including fractals. We study a variety of scenarios depending on the relative orientation of the gradient of film thickness and the stretching direction. In particular, we characterize and rationalize the distribution of singular events in our problem where wrinkles merge to allow a variation of the average value of the wrinkles wavelength across the sample.

1 Introduction

A rigid thin film bounded to a compliant substrate subject to in-plane compression may buckle past a critical value. This instability yields periodic structures similar to those observed in skin wrinkles¹, fingerprints², brain convolutions³, drying green peas^{4,5} and guts⁶. Surface buckling patterns such as periodic wrinkles^{7–9}, ridges^{10,11}, creases^{12,13} or folds^{14,15} in bilayer systems have drawn considerable attention in recent years. In particular they are studied for their potential applications in engineering settings, *e.g.* tunable wetting¹⁶, smart adhesion¹⁷, DNA manipulation¹⁸, photonic structures¹⁹ or microlens array fabrication²⁰. While perfectly periodic structures are the norm, exceptions do exist. Smooth variations of the wrinkling wavelength were obtained by locally varying the stiffness distribution^{21,22} or the thickness of the film^{23,24}. The mismatch of adjacent wrinkles wavelength introduce localized defects – two adjacent ridges merging into a single ridge or a ridge that ends brutally²⁵. These singular points are reminiscent of the structures found in thin sheets under boundary confinement^{26,27}. Such defects are at the origin of the main features of our fingerprints, called minutiae, that are used for identification for biometric applications²⁸.

Here we introduce a simple and robust methodology to fabricate elastic bilayers that present a smooth variation in thickness, thereby enabling us to study wrinkles patterns in non-uniform films. The thin film is obtained via the drainage of a polymeric

coating applied on a uniaxially prestretch substrate, which then cures, thus capturing the structure of the flow. Working in the lubrication limit, we derive the expression for the thickness of this thin layer, which accounts for the rheological properties of the polymeric liquid. When the prestretch is released we observe the apparition of wrinkles and characterize their organization. The wavelength of the pattern they form is compared with the classic theory for Neo-Hookean film-substrate bilayers. When the gradient of film thickness is parallel to the direction of stretching, we find that the wavelength increases continuously from the thinner to the thicker portion of the sample. Conversely, when those directions are orthogonal, we observe the occurrence of merging events. These discrete events appear at the boundary between wrinkles with mismatched wavelength. We recast the classic theory for wrinkles in order to account for the variation in film thickness. Using this scaling, we rationalize the spatial distribution of merging events, their number and size. The self-similarities in the problem suggest that the pattern is fractal, an hypothesis that we test using our experimental data.

2 Experimental protocol

In Fig. 1a, we present a schematic that illustrates our approach. A soft elastic foundation (*i*) is stretched uniaxially to twice its initial length (*ii*). The stretched substrate makes an angle θ with the horizontal and is coated with a thin viscous film that drains under the effect of gravity (*iii*). The drainage results in a smooth, yet non-uniform coating. The thickness of the thin film (apparent in green) increases with the distance, x , from the top of the sample. Upon curing the film creates an elastic layer that is stiffer than

^a Department of Chemical and Biological Engineering, Princeton University, Princeton, New-Jersey 08540, USA.

* To whom correspondence should be addressed: pbrun@princeton.edu

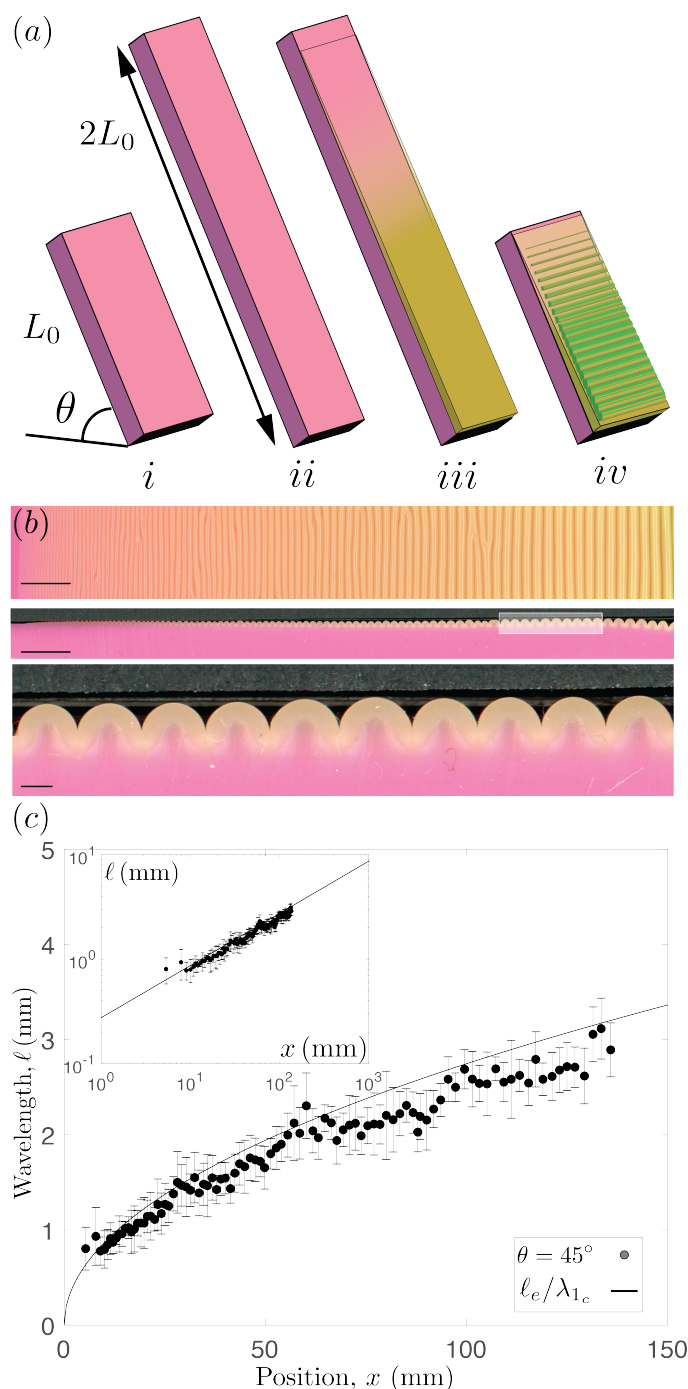


Fig. 1 (a) Sketch of the experimental setup. A soft substrate (pink) is stretched and then coated with a relatively stiffer polymer (green). After the polymer is cured, the stretching is released so as to compress the stiff film. (b) Photographs of a sample in stage *iv*. Shown are the top view and cross section (scale bar indicates 1 cm). Close up: scale bar indicates 1 mm. (c) Variation of the wavelength of the wrinkles with the position x . This particular case corresponds to a tilting angle $\theta = 45^\circ$. (Inset) Log-log representation of the same data.

its foundation. Note that this thin film is stress-free in its original configuration. The substrate is then gradually relaxed and, as the pre-stretch is released, the thin film is compressed (*iv*). Wrin-

kles appear above a compression threshold. In Fig. 1b, we show photographs of our sample after it has been fully relaxed. The top view and the cross-section show the variation of the wrinkle geometry across the sample. The cross-section reveals the non-symmetric shape of the wrinkles that deviate from a sinusoidal shape. In particular, the grooves are sharp and we noticed localized plastic deformations in these areas that persist even when the substrate is stretched again.

In our experiment the thin film is constituted of VPS Elite 32 (Vinyl Polysiloxane, Elite Double 32, Zhermack), while the softer foundation is constituted of VPS Elite 8 (Elite Double 8, Zhermack). Both polymers are mixed at room temperature (20°C) with a base/cure ratio 1:1 in weight for 10 s at 2,000 r.p.m. (clockwise), and then 10 s at 2,200 r.p.m. (counterclockwise). As the film directly polymerizes on the substrate, the layer and the substrate present a strong adhesion such that no delamination between film and substrate has been observed.

The deformation in the substrate is characterized by its principal stretch ratio, $\lambda_1 = L/L_0 > 1$, defined as the ratio between L , the deformed length of the foundation and L_0 , the initial length of the foundation. In the two other principal directions we have $\lambda_2 = \lambda_3 = 1/\sqrt{\lambda_1}$. In Figure 1a-ii we have $\lambda_1 = \lambda_{1_0} = 2$, where λ_{1_0} denotes the initial stretch in the substrate. When the pre-stretch of the substrate is released, the film is under compression. The uniaxial compressive strain $\epsilon_f = (L - 2L_0)/(2L_0) = \lambda_1/2 - 1 < 0$. In our experiments, the pre-stretch is released at a slow rate, $d\lambda_1/dt \sim -0.03\text{s}^{-1}$, so that the wrinkle formation is considered to be quasi-static. The sample is then imaged with a high resolution scanner, the image is binarized and the wavelength of the structure is extracted and averaged along the width of the sample. In Fig. 1c we plot the wavelength ℓ against the position x for a bilayer obtained with a tilting angle $\theta = 45^\circ$ and a initial stretch $\lambda_{1_0} = 2$. The wavelength of the wrinkles continuously increases with the distance from the pouring front and scales with $x^{1/2}$ as illustrated in the logarithmic plot in inset. We now turn to rationalize the selection of the film thickness by considering the drainage of the viscous film on an inclined plane.

3 Film thickness: drainage and curing of the viscous film on an inclined plane

We characterize and model the selection mechanism of the stiff film profile, considering the configuration sketched in Fig. 2a. To this end, we investigate the drainage dynamics coupled to the curing of the polymeric coating. In this section we use transparent acrylic plates as substrates to ease our experimental investigation of the profiles and enable the measurement of the coating thickness using optical transmittance methods²⁹.

VPS Elite 32 is poured on an inclined plate, tilted at an angle θ from the horizontal (see Fig. 2a). A large volume of polymer is used to completely wet the sample and thus avoid any fingering instabilities at the advancing front of the flow. The liquid drains and polymerizes in finite time, yielding an elastic film with a nonuniform thickness. The resulting layers obtained in our experiments for various tilting angles display a continuous variation of the transmittance, thicker films indeed appear darker than rela-

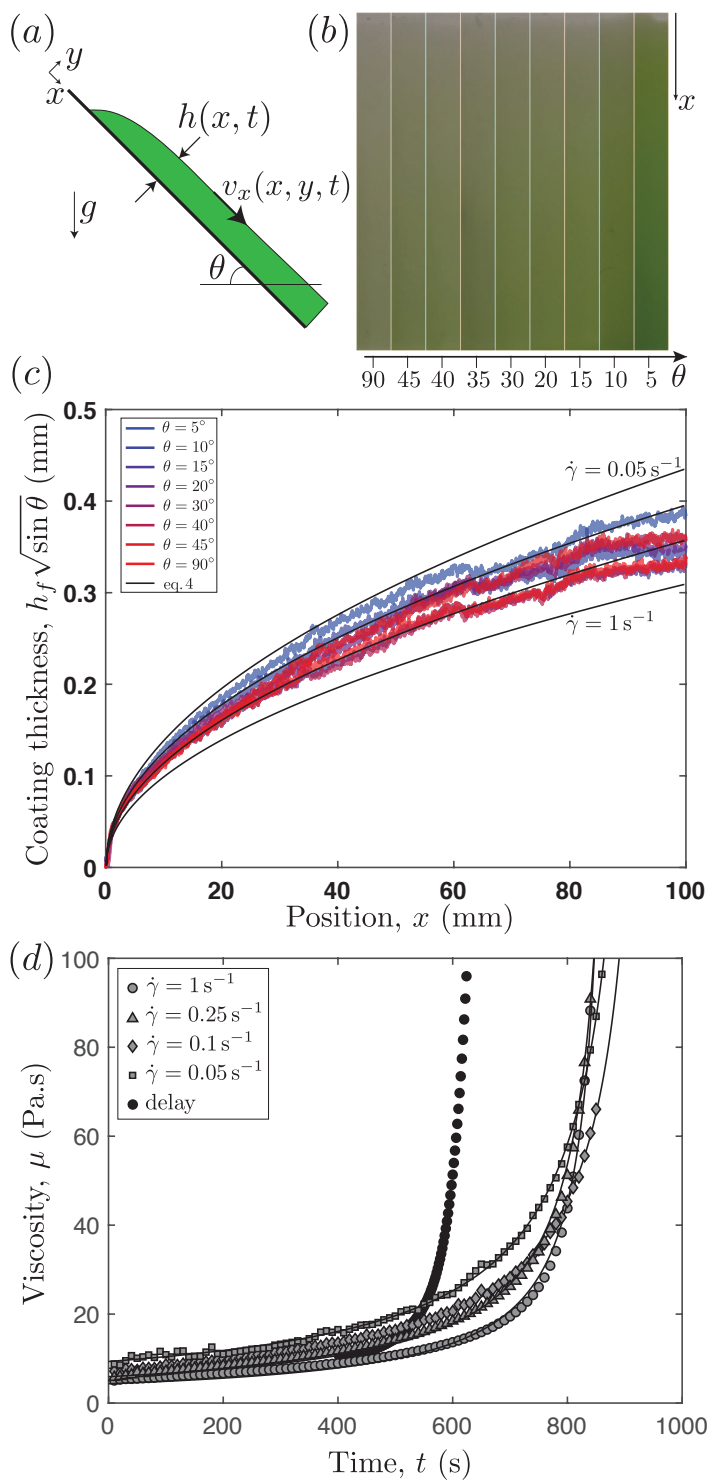


Fig. 2 (a) Sketch of the geometry of the drainage problem. (b) Photographs of 9 samples, obtained with different tilt angles θ . (c) Variation of the final thickness h_f with the position x for different tilt angles θ . The solid black line corresponds to the theoretical prediction from eq. 4. (d) Polymer viscosity over time for 4 different shear rates with corresponding fit (solid black lines). The black circles correspond to an experiment in which the shearing was started after a delay of 400 s.

tively thinner films (Fig. 2b). In our experiments, we observe that

the film thickens with the position, x , and that, overall, thicker films are obtained when the substrate is held closer to the horizontal (small θ). The variation of the optical transmittance with the layer thickness is calibrated on uniform films of known thicknesses obtained by spin-coating. The final thickness of the elastic film, $h_f(x)$, is then extracted from our samples. In Fig. 2c we show that the spatial variation of film thickness across 8 samples can be collapsed by multiplying the film thickness by $\sqrt{\sin \theta}$.

Starting from the lubrication equation to describe the drainage, and neglecting surface tension effects³⁰, we find that the pressure through the film is $P = \rho g \cos \theta (h - y) + P_0$, where ρ is the fluid density, g the acceleration of gravity, P_0 the atmospheric pressure and h the film thickness. Assuming that $\partial_x P \ll \rho g \sin \theta$ or equivalently $\partial_x h \ll \tan \theta$, we find that the velocity field in the x -direction is parabolic. We indeed have $v_x = \rho g \sin \theta / (2\mu) y(2h - y)$, where μ is the viscosity of the fluid assumed to be constant as a first approximation. Using the expression for v_x to evaluate the flow rate $Q = \int_0^h v_x dy$, and then using mass conservation $\partial_t h = -\partial_x Q$ we find that $\partial_t h = -\rho g \sin \theta / \mu h^2 \partial_x h$. Injecting $h(x/t^\alpha)$ in this equation one finds $\alpha = 1$ and the self-similar solution:

$$h(x/t) = \sqrt{\frac{\mu x}{\rho g \sin \theta t}}, \quad (1)$$

whose domain of validity has to be established (indeed eq 1 does not carry any trace of the initial conditions of the problem). In the idealized case where the initial condition of the film is uniform with thickness h_0 the film thickness is a piecewise function. The solution in eq. 1 propagates from $x = 0$ with front speed $\rho g \sin \theta h_0^2 / \mu$, and matches the uniform film solution $h(x,t) = h_0$, which persists from $x = \rho g \sin \theta h_0^2 t / \mu$ to the end of the sample $x = 2L_0$. In practice, we argue that eq. 1 is thus valid across the sample for times greater than $2L_0 \mu / (\rho g \sin \theta h_0^2)$, where h_0 measures of the typical thickness of the initial coating. Eq. 1 is consistent with the scaling in $\sqrt{\sin \theta}$ observed in Fig. 2c, here rationalized as $g \sin \theta$ is the effective gravity of the problem. With a constant fluid viscosity, however, the model predicts a vanishing film thickness as $h \sim t^{-1/2}$. To account for the curing of the polymeric solution that freezes the flow³¹, we consider the evolution of the viscosity of the polymer (see Fig. 2d). The polymer indeed cures in finite time and the viscosity progressively increases as:

$$\mu(t) = \frac{\mu_0}{1 - t/\tau_c} \quad (2)$$

where μ_0 and τ_c are two fitting parameters representing the initial viscosity and the time at which the dynamic is frozen (i.e. when the viscosity diverges). We generalize the solution in eq. 1 to account for the viscosity model in eq. 2:

$$h(x,t) = \sqrt{\frac{x}{\rho g \int_0^t \frac{dt}{\mu(t)} \sin \theta}}. \quad (3)$$

Note that this solution is no longer self similar. Yet, setting $t = \tau_c$, we can estimate the final film thickness:

$$h_f(x) = \sqrt{\frac{2\mu_0 x}{\rho g \sin \theta \tau_c}} \quad (4)$$

To best represent our experiment, the rheology of the polymer mixture is measured under a rheometer for various shear rates that best represent the experiment ($\dot{\gamma} = [0.05, 0.1, 0.25, 1]s^{-1}$). The VPS is found to be slightly shear-thinning³¹, such that μ_0 , as defined in eq. 2, decreases when $\dot{\gamma}$ increases ($\mu_0 = [9.34, 7.81, 5.93, 4.37]Pa.s$) while τ_c remains roughly constant ($\tau_c = [952, 965, 899, 885]s$). The curing time τ_c however decreases significantly in quiescent conditions. This is evident in Fig. 2d: the curing time measured under a constant shear-rate of $\dot{\gamma} = 1s^{-1}$ (open circles) is significantly larger than the one observed for the same shear rate only applied to the mixture after 400 s (black circles). In our experiments, the shear rate varies across the thickness of the sample, in the direction of flow and over time. Additionally, the mixtures are poured at times that may vary slightly from sample to sample, therefore having an effect on the effective value of τ_c . For those reasons, we compare our experimental data to a batch of curves (solid lines in Fig. 2c) corresponding to the aforementioned shear rates. Using such criteria, the model is found to be in reasonable agreement with the experiments. In summary, we have fabricated and rationalized non-uniform coatings. Next, we utilize these profiles to predict the wavelength of the wrinkles.

4 Wavelength selection.

Three scenarios of increasing complexity are considered. Case 1: a film of uniform thickness of VPS Elite 32 is spin-coated on the VPS Elite 8 substrate, which is then stretched to a stretch ratio $\lambda_{1_0} = 2$ (uniform coating as sketched in Fig. 3a). The coating thickness is uniform and h_f is directly measured on the cross-section of the sample. The film thickness can be tuned by varying the spin-coater rotation speed. Case 2: the substrate is first stretched to $\lambda_{1_0} = 2$, then coated with a film of VPS Elite 32, and finally oriented such that the stretching direction is parallel to the direction of drainage (see Fig. 3a). Case 3: the substrate is first stretched to $\lambda_{1_0} = 2$, then coated with a film of VPS Elite 32, and finally oriented such that the stretching direction is orthogonal to the direction of drainage (see Fig. 3a). In all cases, we wait for polymerization before the substrate is relaxed and find that the wrinkling instability appears above a critical compressive strain in the film $\epsilon_{f_c} = \lambda_{1_c}/2 - 1 = -0.35$, or equivalently $\lambda_{1_c} = 1.3$. In Fig. 3b, we report the wrinkling wavelength measured in our bilayer system, shown as a function of the film thickness. Each reported data point is the average value of three independent samples. The wavelength is extracted when the substrate is completely released. Beyond threshold, we assume that the wrinkles grow as stretching continues to be released in such a way that the curvilinear length of the free surface is conserved¹⁵. As a result, the wavelength varies as: $\ell = \ell_c/\lambda_{1_c}$ at leading order.

In case 1 the wavelength (black squares in Fig. 3a) is found to be in favorable agreement with the prediction for a Neo-Hookean film deposited on a stretched Neo-Hookean substrate¹⁰:

$$\ell_e = 2\pi h_f \left(\frac{2}{3} \frac{1}{\lambda_{1_0}^{1/2} (1 + \lambda_{1_0}^{3/2})} \frac{\mu_f}{\mu_s} \right)^{1/3} \quad (5)$$

where $\mu_f = 330kPa$ and $\mu_s = 75kPa$ are the shear modulus of the

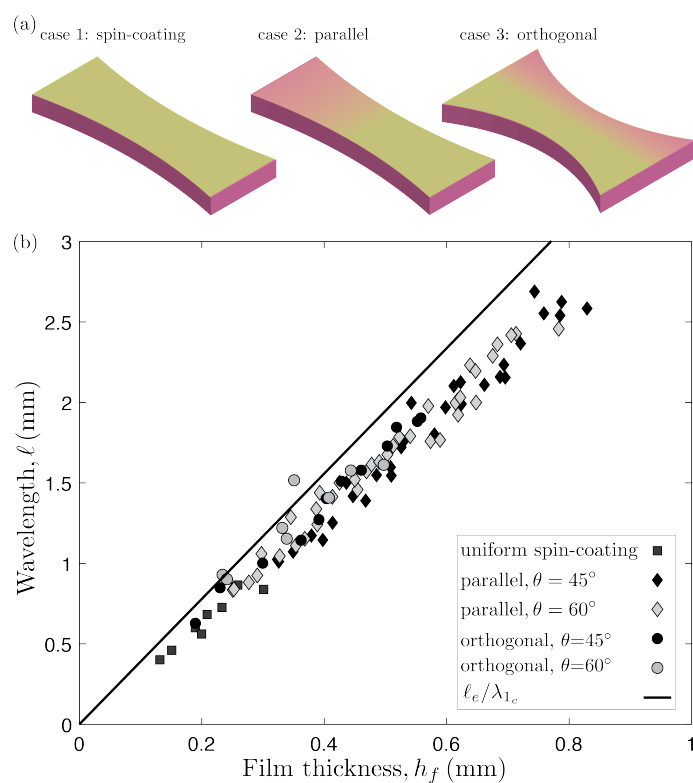


Fig. 3 (a) Sketch of the thickness gradient obtained with spin-coating (case 1), draining in a direction parallel (case 2) or orthogonal (case 3) to the direction of stretching. The substrate appears in pink, while the green gradient represents the variation of the film thickness. (ii) Wrinkle wavelength ℓ versus film thickness h_f obtained for case 1,2,3 and various tilt angles. The solid line corresponds to the theoretical prediction in eq. 5 taking into account the correction ℓ_e/λ_{1_c} due to the compression after the wrinkles appear.

film and the substrate, respectively. The material properties of the film and the substrate are assumed to be isotropic. The shear modulus $\mu_i = E_i/2(1 + \nu_i)$ is a function of the Young modulus E_i and the Poisson ratio ν_i .

In cases 2 and 3, we use eq. 4 to predict the film thickness and compute ℓ_e as defined in eq. 5. The resulting value is found to compare favorably with the wavelength of the wrinkles obtained experimentally with a tilt angle $\theta = 45^\circ$ (dark diamonds and circles) and $\theta = 60^\circ$ (light diamonds and circles in Fig. 3a). We note that the prediction of the spatial variation of the wavelength (eq. 5) is formally derived for a film of constant thickness, an infinitely deep and wide substrate and in the asymptotic limit $\mu_f/\mu_s \gg 1$ (soft foundation and stiff film). In all our experiments, the film thickness is at least 10 times thinner than the substrate, yet the shear modulus of the film is only slightly larger than 4 times the shear modulus of the substrate. Our setup also deviates from the idealized theoretical problem in that the film thickness is not uniform. Yet, we find that the asymptotic expression eq. 5 describes our results favorably.

In the following section, we study the way the system accommodates the evolution of film thickness, especially in the orthogonal case, so as to produce a smooth variation of the wavelength.

In particular, we are interested in the occurrence of merging events, here seen as a regularization mechanism.

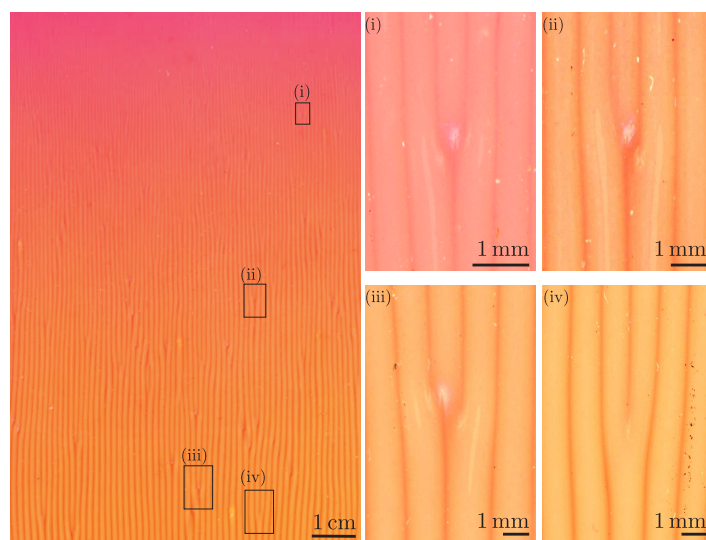


Fig. 4 Photograph of the wrinkle pattern obtained when pouring in a direction orthogonal to that of stretching (and with inclination $\theta = 45^\circ$). Close-up of the merging events at different length scales: 3 wrinkles merging into 2 wrinkles (i-iii) and 2 wrinkles merging into 1 wrinkle (iv).

5 Merging events and self-similarity

We turn to describe the geometry and density of the merging events in case 3, *i.e.* when the stretching direction is orthogonal to the flow (see Fig. 3a). In Fig. 4, we show a photograph of a sample, that has been stretched in the horizontal direction, while the flow was vertical, from top to bottom. Due to the continuous variation in film thickness, small wavelengths (at the top of the sample) merge to match larger wavelengths (at the bottom of the sample). The size mismatch of adjacent wrinkles introduces localized defects where the wrinkles merge²⁵. We find two types of merging events: 3 wrinkles merging into 2 wrinkles (Fig. 4(i) – (iii)) and 2 wrinkles merging in 1 wrinkle (Fig. 4(iv)). In both cases, the size of the singularity²⁷ where one groove vanishes is small enough such that the merging events appear to be self-similar. Shown in Fig. 4(i) – (iii) are close up photographs of three merging events that have been rescaled by the wavelength of the wrinkles shortly after the singularity, and which appear qualitatively identical. In all cases, we notice that the wrinkle that vanishes appears to be smaller than its neighbors. To further investigate the structure of the wrinkled pattern we turn to quantitative analysis.

The position of the ridges and the merging events are automatically detected using an in-house Python algorithm, that leverages the change in intensity of the sample and the directionality of the wrinkles. In Fig. 5a, we show a typical outcome of our routine. Shown in black are the edges detected by the algorithm, while red triangles show merging events, M . Conversely blue triangles indicate the "birth of a wrinkle" that is the point where a groove appears, B . They correspond to cases where a groove ends, while another one appears next to it, as if the wrinkle was shifting lo-

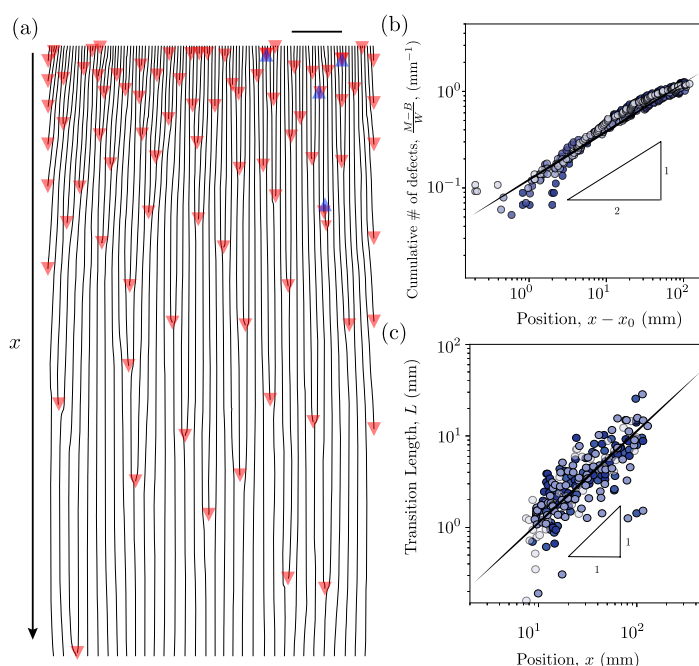


Fig. 5 (a) Position of the wrinkles and merging events extracted from the photograph of a sample. Red triangles indicate the position of merging events (M) while blue triangles indicate points where a groove appears (B). Scale bar indicates 1 cm. (b) Cumulative number of defects as a function of the distance $x - x_0$, where x_0 is the position of the first detected merging event. (c) Shown is the linear relation between the transition length L and the distance to the origin x .

cation. We find that there are a larger number of merging events at the top (thin region, small wavelength) than at the bottom (thick region, large wavelength). In Fig. 5b, we report the cumulative number of such merging events, $(M - B)/W$ for four different samples, where W is the width of the sample. We find that $(M - B)/W \sim \sqrt{x - x_0}$, where x_0 is the position of the first merging detected. This result is consistent with the scaling of the wavelength $\ell \sim \sqrt{x}$ and indicates that merging is the main mechanism that drives the overall variation of wavelength across the sample. Yet, as merging are discrete events, we expect to find some areas of frustration in the pattern. In fact, we observe that wrinkles deviate from their nominal wavelength before merging (see Fig 4). We define L as the distance from a singularity over which the wavelength is less than 90% of the mean wavelength, $\bar{\ell}(x)$, averaged across the width of the sample. Leveraging on the fact that merging are localized events²⁷, we expect that $d\ell/dx \sim \ell/L$. Considering the scaling, $\ell \sim \sqrt{x}$, we conclude that $L \sim x$. This scaling is in agreement with the results shown in Fig. 5c. This level of self-similarity suggests that the pattern might be fractal.

To further characterize the spatial organization of the wrinkles pattern, we compute the fractal dimension via a box counting method based on the position of the ridges. We place our skeletonized sample on an evenly spaced grid and count how many boxes are required to cover the set³². Shown in Fig. 6a are the areas obtained with those boxes for three different box sizes. Boxes that have an intersection with the ridges are colored in gray, while others are left white. In Fig. 6b we plot the number of such boxes

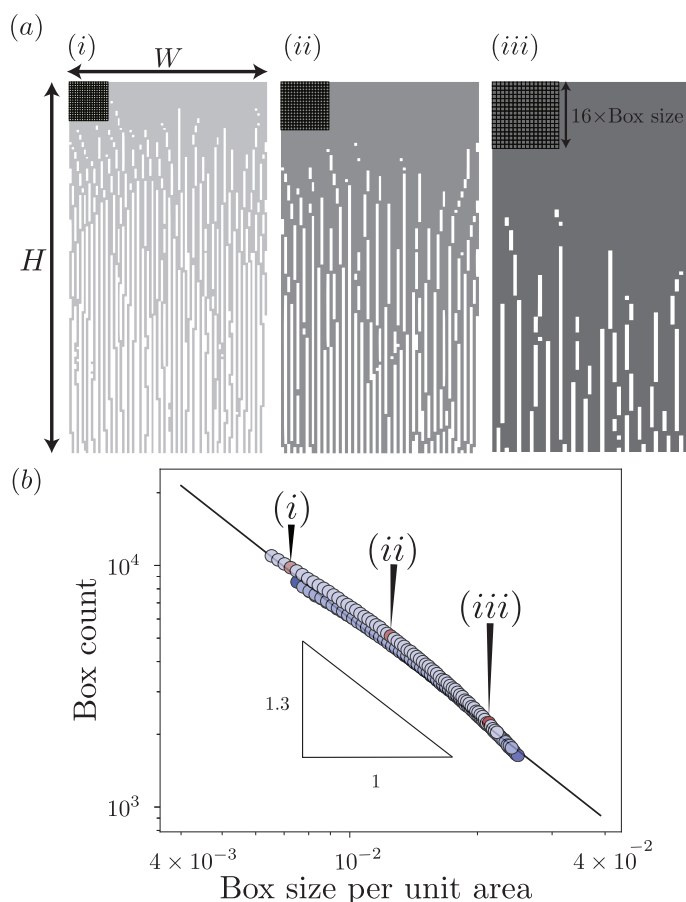


Fig. 6 (a) Result of the box counting method applied on the same sample for three different box size. A gray pixel in the image indicates a pixel with an intersection with a ridge. Conversely, white pixels indicate no intersection. (b) Number of boxes as a function of the box size for five different samples.

as a function of their size for four different samples. We find that the data gathered from our samples collapse on a single curve, such that we conclude that the pattern is indeed fractal with dimension 1.3. This fractal dimension is thus larger than that of a line (dimension 1) and far less than that of a space filling curve (dimension 2), a value close to that of several natural patterns³³. This dimension is a response of the system to the variation of film thickness imposed by the flow, in a way its fingerprint. In the remainder of the paper, we seek to identify ways to force the system away from its natural wavelength and quantify the robustness of the wrinkling instability.

6 Forcing the instability away from the elastic wavelength

We propose a perturbative approach to force the instability away from the elastic wavelength. Instead of a smooth substrate, we introduce some features at the surface of the pre-stretched foundation (see Fig. 7a). Such modulations are obtained using a laser cutter to engrave the base of the mold in which the sample is prepared. Rectangular crenel shapes of varying wavelength ℓ_R , width 0.5 mm and amplitude 0.3 mm are created in the center of

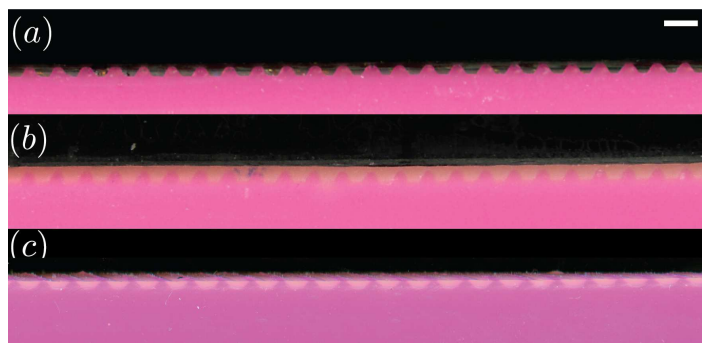


Fig. 7 (a) Grooves are etched at the surface of the substrate. (b) The sample is then coated and (c) stretched. Scale bar 1mm.

the sample, while the remainder of the sample remains smooth. The soft substrate is then coated with a uniform film of VPS Elite 32 using a spin-coater (cross-section of the sample in Fig. 7b). The substrate is finally stretched uniaxially before polymerization (Fig. 7c). Upon curing, the stretch is released and wrinkles appear across the sample. We found that we were able to force the wavelength of those wrinkles in a certain range. We define ℓ_N , the natural wavelength obtained without forcing ($\ell_N \simeq \ell_e/1.3$). Here, we find that forcing in the range $1 < \ell_R/\ell_N < 1.8$ is effective, while values outside of this range lead to a variety of issues, *e.g.* period doubling. In all cases, we find that when moving sufficiently far from the center of the sample the wrinkles returned to their natural wavelength ℓ_N .

For the cases in the range $1 < \ell_R/\ell_N < 1.8$, we characterize the transition between the imposed wavelength ℓ_R and the elastic one ℓ_N . Fig. 7a shows three cross-sections cut at a position $x = 2.5$ (i), 6 (ii) and 15 (iii) mm away from the center of the sample (the forcing in this case is $\ell_R = 1.6\ell_N$). In the area of the sample where the substrate thickness is modulated, we observe that the wavelength corresponds to the forcing value ℓ_R (cross-section (i) in Fig. 8a). The wavelength then decreases as one moves away from center (cross-section (ii)) and eventually returns to its natural value ℓ_N (cross-section (iii)). In Fig. 8b, we plot the variation of the wavelength for five samples forced at different wavelengths. While imposing a wavelength far from the natural elastic wavelength leads to a brutal transition from ℓ_R to ℓ_N , forcings closer to the natural elastic wavelength presents a smoother transition toward ℓ_N . To characterize this regularization, we measure the distance Δx for which the wavelength returns within 20% of its natural value. The evolution of Δx with ℓ_R is shown in the inset of Fig. 8b in semilog scale. We found that this evolution is coherent with an exponential decrease $\Delta x/\ell_N \sim \exp(-\zeta \ell_R/\ell_N)$ where $\zeta = 5.0$ is a numerical factor. We note that the typical lengthscale of the exponential decay $\ell_N/5$ is smaller than ℓ , indicating the fast decay of the wavelength towards the value of the natural wavelength of the system. Wrinkling is thus particularly robust and the size of the wrinkles is mostly defined locally by the thickness of the substrate.

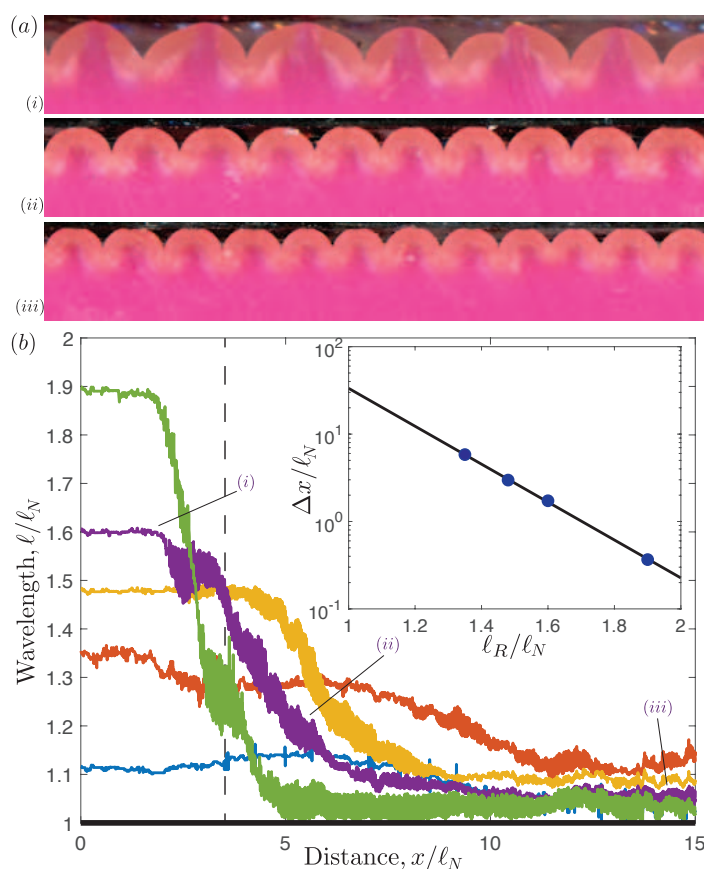


Fig. 8 (a) Cross-sections of the wrinkling profile in a sample forced at $\ell_R = 1.6\ell_N$ captured at a distance $x = 2.5$ (i), 6 (ii) and 15 (iii) mm away from the center of the sample. (b) Spatial variation of the wavelength ℓ normalized by the natural wavelength ℓ_N for five different imposed wavelength ℓ_R . The width of the perturbation (3 mm) is indicated by the vertical dashed line. (Inset) Regularization distance Δx , defined as the distance between the edge of the perturbation and the point for which the wavelength returns to $1.2\ell_N$.

7 Conclusion

In summary, we have systematically explored the wrinkling pattern obtained with a smooth variation of the film thickness, based on the drainage of a viscous film on a pre-stretched substrate. We found that the wavelength is everywhere imposed by the coating thickness. In particular, the mismatch of adjacent wavelengths introduces localized defects where the wrinkles merge. We found that the number of those defects scales with the wavelength and that the pattern they form is fractal. By forcing the instability away from its natural wavelength using a perturbative approach, we found that regularization length after which the structure relaxes back to its natural state is small, confirming the robustness of the instability.

Acknowledgments:

This work was supported by the National Science Foundation, Princeton University Materials Research Science and Engineering Center DMR-1420541.

References

- 1 G. Limbert and E. Kuhl, *Soft matter*, 2018, **14**, 1292–1300.
- 2 M. Kücken and A. Newell, *EPL (Europhysics Letters)*, 2004, **68**, 141.
- 3 T. Tallinen, J. Y. Chung, F. Rousseau, N. Girard, J. Lefèvre and L. Mahadevan, *Nature Physics*, 2016, **12**, 588.
- 4 B. Li, F. Jia, Y.-P. Cao, X.-Q. Feng and H. Gao, *Physical Review Letters*, 2011, **106**, 234301.
- 5 J. Marthelot, P.-T. Brun, F. L. Jiménez and P. M. Reis, *Physical Review Materials*, 2017, **1**, 025601.
- 6 A. E. Shyer, T. Tallinen, N. L. Nerurkar, Z. Wei, E. S. Gil, D. L. Kaplan, C. J. Tabin and L. Mahadevan, *Science*, 2013, **342**, 212–218.
- 7 H. Allen, *Analysis and Design of Structural Sandwich Panels*, Pergamon Press (New York), 1969.
- 8 F. Brau, H. Vandeparre, A. Sabbah, C. Poulard, A. Boudaoud and P. Damman, *Nature Physics*, 2011, **7**, 56–60.
- 9 Y. Ebata, A. B. Croll and A. J. Crosby, *Soft Matter*, 2012, **8**, 9086–9091.
- 10 Y. Cao and J. W. Hutchinson, *Journal of Applied Mechanics*, 2012, **79**, 031019.
- 11 A. Takei, L. Jin, J. W. Hutchinson and H. Fujita, *Advanced Materials*, 2014, **26**, 4061–4067.
- 12 S. Cai, D. Chen, Z. Suo and R. C. Hayward, *Soft Matter*, 2012, **8**, 1301–1304.
- 13 R. Al-Rashed, F. L. Jiménez, J. Marthelot and P. M. Reis, *Soft Matter*, 2017, **13**, 7969–7978.
- 14 L. Pocivavsek, R. Dellsy, A. Kern, S. Johnson, B. Lin, K. Y. C. Lee and E. Cerda, *Science*, 2008, **320**, 912–916.
- 15 F. Brau, P. Damman, H. Diamant and T. A. Witten, *Soft Matter*, 2013, **9**, 8177–8186.
- 16 C. Cao, H. F. Chan, J. Zang, K. W. Leong and X. Zhao, *Adv. Mater.*, 2014, **26**, 1763–1770.
- 17 E. P. Chan, E. J. Smith, R. C. Hayward and A. J. Crosby, *Advanced Materials*, 2008, **20**, 711–716.
- 18 S. Nagashima, H. D. Ha, A. Košmrlj, H. A. Stone and M.-W. Moon, *Proceedings of the National Academy of Sciences*, 2017, 201700003.
- 19 J. B. Kim, P. Kim, N. C. Pégard, S. J. Oh, C. R. Kagan, J. W. Fleischer, H. A. Stone and Y.-L. Loo, *Nature Photonics*, 2012, **6**, 327.
- 20 E. P. Chan and A. J. Crosby, *Advanced Materials*, 2006, **18**, 3238–3242.
- 21 Y. Ni, D. Yang and L. He, *Physical Review E*, 2012, **86**, 031604.
- 22 J. Wang, B. Li, Y.-P. Cao, X.-Q. Feng and H. Gao, *Applied Physics Letters*, 2016, **108**, 021903.
- 23 J. Yin and X. Chen, *Philosophical Magazine Letters*, 2010, **90**, 423–433.
- 24 S. Yu, Y. Ni, L. He and Q.-L. Ye, *ACS Applied Materials & Interfaces*, 2015, **7**, 5160–5167.
- 25 B. A. Glatz, M. Tebbe, B. Kaoui, R. Aichele, C. Kuttner, A. E. Schedl, H.-W. Schmidt, W. Zimmermann and A. Fery, *Soft Matter*, 2015, **11**, 3332–3339.

- 26 R. D. Schroll, E. Katifori and B. Davidovitch, *Physical Review Letters*, 2011, **106**, 074301.
- 27 H. Vandeparre, M. Piñeirua, F. Brau, B. Roman, J. Bico, C. Gay, W. Bao, C. N. Lau, P. M. Reis and P. Damman, *Physical Review Letters*, 2011, **106**, 224301.
- 28 H. J. Bae, S. Bae, C. Park, S. Han, J. Kim, L. N. Kim, K. Kim, S.-H. Song, W. Park and S. Kwon, *Advanced Materials*, 2015, **27**, 2083–2089.
- 29 F. López Jiménez, S. Kumar and P. M. Reis, *Advanced Optical Materials*, 2016, **4**, 620–626.
- 30 E. Guyon, J.-P. Hulin, L. Petit and C. D. Matescu, *Physical hydrodynamics*, Oxford university press, 2001.
- 31 A. Lee, P.-T. Brun, J. Marthelot, G. Balestra, F. Gallaire and P. Reis, *Nature communications*, 2016, **7**, 11155.
- 32 K. Falconer, *Fractal geometry: mathematical foundations and applications*, John Wiley & Sons, 2004.
- 33 B. B. Mandelbrot, *The fractal geometry of nature*, WH Freeman New York, 1983.